0026-895X/06/7003-878–886$20.00
MOLECULAR PHARMACOLOGY
Copyright © 2006 The American Society for Pharmacology and Experimental Therapeutics
Mol Pharmacol 70:878–886, 2006

Vol. 70, No. 3
26427/3134173
Printed in U.S.A.

Broad Specificity of Mammalian Adenylyl Cyclase for Interaction with 2′,3′-Substituted Purine- and Pyrimidine Nucleotide Inhibitors[S]

Tung-Chung Mou, Andreas Gille,[1] Srividya Suryanarayana, Mark Richter, Roland Seifert, and Stephen R. Sprang

Department of Biochemistry, University of Texas Southwestern Medical Center at Dallas, Dallas, Texas (T.-C.M., S.R.S.); Department of Pharmacology and Toxicology, the University of Kansas, Lawrence, Kansas (A.G., R.S.); Department of Molecular Biosciences, the University of Kansas, Lawrence, Kansas (S.S., M.R.); and Department of Pharmacology and Toxicology, University of Regensburg, Regensburg, Germany (R.S.)

Received May 8, 2006; accepted June 8, 2006

ABSTRACT

Membrane adenylyl cyclases (mACs) play an important role in signal transduction and are therefore potential drug targets. Earlier, we identified 2′,3′-*O*-(*N*-methylanthraniloyl) (MANT)-substituted purine nucleotides as a novel class of highly potent competitive mAC inhibitors (K_i values in the 10 nM range). MANT nucleotides discriminate among various mAC isoforms through differential interactions with a binding pocket localized at the interface between the C1 and C2 domains of mAC. In this study, we examine the structure/activity relationships for 2′,3′-substituted nucleotides and compare the crystal structures of mAC catalytic domains (VC1:IIC2) bound to MANT-GTP, MANT-ATP, and 2′,3′-(2,4,6-trinitrophenyl) (TNP)-ATP. TNP-substituted purine and pyrimidine nucleotides inhibited VC1:IIC2 with moderately high potency (K_i values in the 100 nM range). Elongation of the linker between the ribosyl group and the MANT group and substitution of *N*-adenine atoms with MANT reduces inhibitory potency. Crystal structures show that MANT-GTP, MANT-ATP, and TNP-ATP reside in the same binding pocket in the VC1:IIC2 protein complex, but there are substantial differences in interactions of base, fluorophore, and polyphosphate chain of the inhibitors with mAC. Fluorescence emission and resonance transfer spectra also reflect differences in the interaction between MANT-ATP and VC1:IIC2 relative to MANT-GTP. Our data are indicative of a three-site mAC pharmacophore; the 2′,3′-*O*-ribosyl substituent and the polyphosphate chain have the largest impact on inhibitor affinity and the nucleotide base has the least. The mAC binding site exhibits broad specificity, accommodating various bases and fluorescent groups at the 2′,3′-*O*-ribosyl position. These data should greatly facilitate the rational design of potent, isoform-selective mAC inhibitors.

Adenylyl cyclases (ACs) catalyze the conversion of ATP to cAMP, a ubiquitous cellular second messenger that regulates a variety of cellular processes including gene transcription, enzyme regulation, and sensory transduction in both prokaryotic and eukaryotic organisms (Sunahara et al., 1996; Hanoune and Defer, 2001). The nine isoforms of mammalian membrane AC (mAC) possess a pair of 2-fold symmetrically arranged class III cyclase homology domains in which catalysis occurs (Linder et al., 1990). mAC isoforms are stimulated by the GTP-bound G protein $G\alpha_s$ and, with the exception of type IX mAC, by the diterpene forskolin (FSK) (Sunahara et al., 1996). The N- and C-terminal cyclase homology domains of mAC, when expressed as independent polypeptides and mixed together are catalytically competent and potently stimulated by FSK and $G\alpha_s$·GTPγS (Whisnant et al., 1996; Sunahara et al., 1997). The three-dimensional structure of a

This work was supported by National Institutes of Health grant DK46371 (to S.R.S.), Welch Foundation grant I-229 (to S.R.S.), the John W. and Rhoda K. Pate Professorship (to S.R.S.), grant 0450120Z from the Heartland Affiliate of the American Heart Association (to R.S.), the Graduate Training Program (Graduiertenkolleg) 760 "Medicinal Chemistry: Molecular Recognition-Ligand-Receptor Interactions" of the Deutsche Forschungsgemeinschaft (to R.S.), and a predoctoral fellowship from the Studienstiftung des Deutschen Volkes (to A.G.).

[1] Current affiliation: Department of Pharmacology, University of Heidelberg, Heidelberg, Germany.

Article, publication date, and citation information can be found at http://molpharm.aspetjournals.org.
doi:10.1124/mol.106.026427.

[S] The online version of this article (available at http://molpharm.aspetjournals.org) contains supplemental material.

ABBREVIATIONS: AC, adenylyl cyclase; mAC, membrane-bound adenylyl cyclase; $G\alpha_s$, stimulatory G-protein for mAC; FSK, forskolin; MP-FSK, 7-acetyl-7-[*O*-(*N*-methylpiperazino)-γ-butyryl)]-forskolin; VC1 and IIC2, the N- and C-terminal catalytic domains from canine type V mAC and rat type II mAC, respectively, expressed as soluble proteins; GTPγS, guanosine 5′-[γ-thio]triphosphate; SVD, singular value decomposition; FRET, fluorescence resonance energy transfer; MABA, 8-[(4-(*N*-methylanthraniloyl)amino)butyl]amino; MAHA, 8-[(6-(*N*-methylanthraniloyl)amino)hexyl]-amino; MANT, 2′(3′)-*O*-(*N*-methylanthraniloyl); 6-MANT, N^6-[6-((*N*-methylanthraniloyl)amino)hexyl]; MANT-EDA, 2,3,-[(2-(*N*-methylanthraniloyl)amino)ethyl-carbamoyl]; TNP, 2′,3′-*O*-(2,4,6-trinitrophenyl).

catalytic heterodimer formed by the C1 domain of type V mAC and the C2 domain of type II mAC (VC1:IIC2), bound to FSK and $G\alpha_s$·GTPγS, has been described previously (Tesmer et al., 1997), as have those of a variety of complexes in which VC1:IIC2 is bound to different ATP analogs (Tesmer et al., 1999, 2000). These crystal structures, together with biochemical data (Dessauer et al., 1997), indicate that ATP binds at one of two pseudosymmetric binding sites at the C1:C2 interface, whereas FSK binds to the pseudo-2-fold–related binding site (Tesmer et al., 1997). The catalytic pocket includes a purine-binding subsite derived from the C2 domain that provides residues that specifically bind to the adenine base of the substrate. A second subsite, composed of residues derived from the βαββαβ motif of the C1 domain, includes a P-loop that accommodates the nucleotide phosphates and a pair of conserved aspartate residues that ligate the metal ion cofactors (Tesmer and Sprang, 1998).

We have discovered that the fluorescent 2′(3′)-*O*-(*N*-methylanthraniloyl) (MANT) derivative of GTP (MANT-GTP) is a highly potent competitive inhibitor of several mAC isoforms as well as of the soluble VC1:IIC2 complex (Gille and Seifert, 2003; Gille et al., 2004). This finding was surprising in view of the high selectivity of mAC toward ATP in preference to GTP as a substrate (Sunahara et al., 1998; Gille et al., 2004). The crystal structure of the VC1:IIC2 complex with MANT-GTP revealed that the MANT nucleotide is bound to the catalytic site in reverse orientation with respect to ATP analogs that are not derivatized with bulky substituents at the 2′(3′) position. In the reverse orientation, the guanine moiety in the purine binding site is accommodated by a pattern of hydrogen bonds analogous to those formed with adenine (Mou et al., 2005). The reverse orientation of MANT-GTP in the catalytic site is a consequence of the intercalation of the MANT moiety into a hydrophobic pocket at the interface between the C1 and C2 domains. Other MANT nucleotides, such as MANT-ATP, also inhibit $G\alpha_s$/FSK-activated VC1:IIC2 with K_i values in the 10 to 100 nM range (Gille et al., 2004). Thus, the catalytic site of mAC exhibits a much lower base specificity toward 2′(3′)-MANT nucleotides than was previously observed for other ATP analogs. The relaxation of specificity may arise from enlargement of the inhibitor-binding pocket as a result of the insertion of the MANT group into the interdomain site.

The forgoing findings prompted us to study in more detail the inhibition of VC1:IIC2 by 2′,3′-substituted purine and pyrimidine nucleotides. In particular, we examined MANT-EDA-ATP, which possesses a longer linker between the ribosyl moiety and the fluorophore, and three analogs (6-MANT-ATP, MABA-ATP, and MAHA-ATP) in which the fluorophore is attached to N6 and N8, respectively, of adenine through various linkers. We also examined 2′,3′-substituted TNP nucleotides, which are widely used for studying conformational changes in proteins (Hiratsuka, 2003). Fluorescence analysis suggested that MANT-GTP and MANT-ATP bind to VC1:IIC2 in slightly different ways, calling for more detailed analysis by X-ray crystallography. In this study, we show that MANT-GTP, MANT-ATP, and TNP-ATP bind to a common site in mAC, but they do so in different ways, as corroborated by fluorescence spectroscopy. These data support the concept that the catalytic site of mAC, if structurally perturbed at the domain interface, shows broad specificity for active site-directed inhibitors. It may be inferred from our data that potent mAC inhibitors can be designed with considerable latitude with respect to the composition of the moieties that fill distinct subsites within the catalytic pocket of the enzyme.

Materials and Methods

Materials. Recombinant adenylyl cyclase cytosolic C1a domain from canine type V (VC1), C2a domain from rat type II (IIC2), and bovine $G\alpha_s$ were purified and stored as described previously (Tesmer et al., 2002). $G\alpha_s$ was activated by incubation with 10 μM GTPγS and 2 mM $MgCl_2$ at 30°C for 1 h, and the resulting $G\alpha_s$ · GTPγS complex was digested by trypsin. Free GTPγS and inactivated $G\alpha_s$ were removed by passing the sample through nickel-nitrilotriacetic acid resin. All MANT nucleotides, TNP-GDP, TNP-GTP, TNP-CTP, and TNP-UTP were obtained from Jena Bioscience (Jena, Germany). TNP-AMP, TNP-ADP, and TNP-ATP were obtained from Invitrogen (Eugene, OR). GTPγS was from Roche (Indianapolis, IN). FSK and MP-FSK were obtained from Calbiochem (La Jolla, CA). Sources of other materials are described elsewhere (Gille and Seifert, 2003; Gille et al., 2004; Mou et al., 2005).

AC Activity Assays. AC activity was determined essentially as described previously (Mou et al., 2005). In brief, reaction mixtures contained 40 μM ATP/Mn^{2+}, 10 mM $MnCl_2$, and MANT nucleotides or TNP nucleotides at concentrations from 1 nM to 1 mM as appropriate to obtain saturated inhibition curves. In addition, assay tubes contained VC1 (8 nM) and IIC2 (40 nM). For experiments with $G\alpha_s$·GTPγS, tubes contained VC1 (3 nM), IIC2 (15 nM), and $G\alpha_s$·GTPγS (51 nM). Reactions were conducted in the presence of 100 μM FSK. After a 2-min preincubation at 30°C, reactions were initiated by adding 20 μl of reaction mixture containing (final) 1.0 μCi/tube [α-^{32}P]ATP, 0.1 mM cAMP, and 100 mM KCl in 25 mM Na^+HEPES, pH 7.4. It should be noted that AC assays were conducted in the absence of an NTP-regenerating system to allow for the analysis of 2′,3′-substituted NDPs and NMPs that would otherwise be phosphorylated to the corresponding NTPs by the regenerating system (Gille et al., 2004). Reactions were conducted for 10 to 20 min at 30°C and were terminated by the addition of 20 μl of 2.2 N HCl. Denatured protein was sedimented by a 1-min centrifugation at 25°C and 15,000*g*. Sixty-five microliters of the supernatant fluid were applied onto disposable columns filled with 1.3 g of type WN-6 neutral, activity grade Super I alumina (Sigma-Aldrich, St. Louis, MO). [^{32}P]cAMP was separated from [α-^{32}P]ATP by elution of [^{32}P]cAMP with 4 ml of 0.1 M ammonium acetate, pH 7.0. Recovery of [^{32}P]cAMP was ~80% as assessed with [^{3}H]cAMP as standard. [^{32}P]cAMP was determined by Čerenkov radiation or liquid scintillation counting using Ecolume scintillation cocktail (Fisher, Pittsburgh, PA). Competition isotherms were analyzed by nonlinear regression using the Prism 4.0 software (GraphPad, San Diego, CA).

Fluorescence Spectroscopy and Data Analysis. All experiments were conducted using a Cary Eclipse fluorescence spectrophotometer equipped with a Peltier-thermostated multicell holder at 25°C (Varian, Walnut Creek, CA). Measurements were performed in a quartz fluorescence microcuvette (Hellma, Plainview, NY). The final assay volume was 150 μl. Reaction mixtures contained a buffer consisting of 100 mM KCl, 10 mM $MnCl_2$, and 25 mM Na^+HEPES, pH 7.4. Steady-state emission spectra were recorded at low speed with λ_{ex} = 350 nm (λ_{em} = 370–500 nm) and λ_{ex} = 280 nm (λ_{em} = 300–500 nm) with 1 μM MANT-GTP or 1 μM MANT-ATP in the absence and presence of 5 μM VC1 plus 25 μM IIC2 without and with 100 μM MP-FSK. Fluorescence recordings were analyzed with the spectrum package of the Cary Eclipse software (Varian, Walnut Creek, CA). Baseline fluorescence (buffer alone) was subtracted. Figure 1 shows superimposed original fluorescence recordings. Similar results were obtained in four independent experiments using two different batches of VC1 and IIC2.

Crystallization, Structure Determination, and Model Refinement for AC Complexes with TNP-ATP and MANT-ATP. A mixture of individually purified recombinant VC1, IIC2, and trypsin-

treated $G\alpha_s$·GTPγS (1.5:1:1) was passed through tandemly arranged Superdex 75 and 200 gel filtration columns (GE Healthcare, Little Chalfont, Buckinghamshire, UK) in the presence of excess MP-FSK and GTPγS. Fractions containing the heterotrimeric complex were collected and concentrated to 8 mg/ml in a buffer of 20 mM Na^+HEPES, pH 8.0, 2 mM EDTA, 2 mM $MgCl_2$, 2 mM dithiothreitol, 100 mM NaCl, 25 μM MP-FSK, and 10 μM GTPγS for crystallization. Adenylyl cyclase protein complex crystals were grown, harvested, and cryoprotected under the conditions described previously (Tesmer et al., 2002; Mou et al., 2005). Before cryoprotection, crystals were soaked in reservoir solution containing 2 mM TNP-ATP or 2 mM MANT-ATP with 3 mM $MnCl_2$ for 2 to 4 h at room temperature and then harvested in cryoprotectant. Cryoprotected crystals were mounted in 0.1- to 0.2-mm loops and stored in liquid nitrogen.

Diffraction data sets were collected by the oscillation method at the Advanced Light Source (ALS) 8.2.1 beamline at Berkeley, CA with an incident beam wavelength of 1.0781Å, and the images were processed with the HKL2000 package (Otwinowski and Minor, 1997). As a result of anisotropy, data with l index >20 for crystals of the TNP-ATP·Mn^{2+} complex and l index >18 for crystals of the MANT-ATP·Mn^{2+} complex were excluded from the data set. Crystals of the protein complex with MANT-ATP·Mn^{2+} or TNP-ATP·Mn^{2+} were nearly isomorphous with those of the VC1:IIC2·FSK: $G\alpha_s$·GTPγS complex (Tesmer et al., 1997). Coordinates of the latter complex with MANT-GTP (Protein Data Bank code 1TL7) were used as the initial phasing model. The inhibitors and metal ions in the structures were located in a SIGMA-A weighted $|Fo| - |Fc|$ difference omit map computed with phases from the refined model. Atomic positions and thermal parameters were refined by successive rounds of rigid body, simulated annealing, Powell minimization, and B factor refinement using the CNS 1.1 program suite (Brunger et al., 1998). The model was iteratively improved by manual refitting into weighted $2|Fo| - |Fc|$ maps using the computer graphics program O (Jones et al., 1991), and subsequent cycles of refinement using CNS. Coordinates for the TNP-ATP·Mn^{2+} and MANT-ATP·Mn^{2+} structures have been deposited in the Protein Data Bank with the codes 2GVD and 2GVZ, respectively.

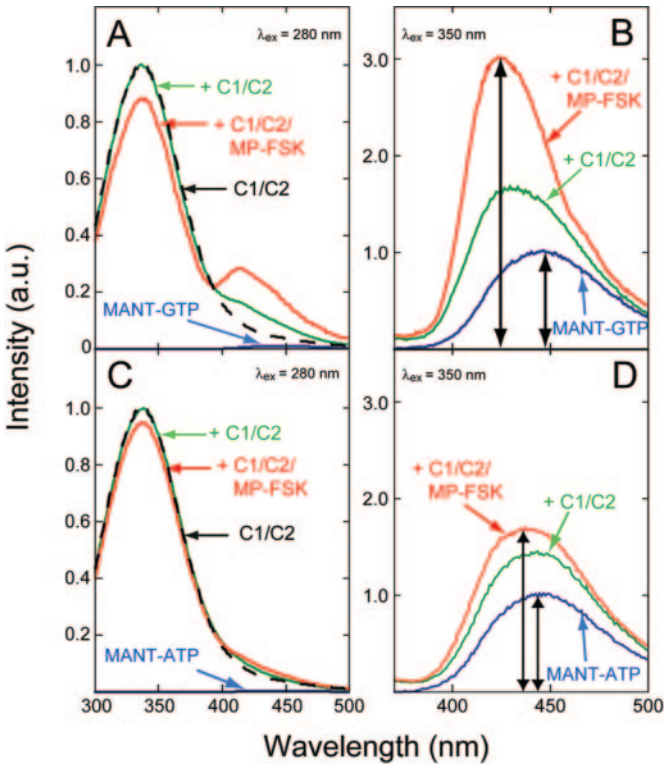

Fig. 1. Fluorescence emission spectra of MANT-GTP and MANT-ATP in the absence and presence of VC1:IIC2 and MP-FSK. Fluorescence measurements were conducted as described under *Materials and Methods*. A and B, measurements with MANT-GTP; C and D, measurements with MANT-ATP. Spectra were recorded at λ_{ex} = 280 nm (λ_{em} = 300–500 nm) in A and C and at λ_{ex} = 350 (λ_{em} = 300–500 nm) in B and D. Cuvettes containing VC1 (5 μM) and IIC2 (25 μM) in the presence of MP-FSK (100 μM) were equilibrated for 10 min at 25°C before recording spectra. MANT-GTP and MANT-ATP were used at a concentration of 1 μM each. Representative fluorescence emission spectra are shown for MANT-GTP/MANT-ATP alone (blue lines) and VC1:IIC2 (C1/C2) only (black dashed lines), MANT-GTP/MANT-ATP in the presence of VC1:IIC2 (green lines) and MANT-GTP/MANT-ATP in the presence of both VC1:IIC2 and MP-FSK (red lines). Fluorescence intensities are shown in arbitrary units (a.u.). The black arrows in B and D indicate the emission maxima for MANT-GTP/MANT-ATP in the absence of VC1:IIC2 and in the presence of VC1:IIC2 plus MP-FSK. Fluorescence tracings are representative for five independent experiments with different protein batches.

Singular Value Decomposition (SVD) Calculation and Error Analysis. For each member, i, of a set of twenty AC inhibitors, inhibitory potency, K_i, was modeled as the sum of the contributions, $\kappa_i(j)$, of the two or three equally weighted chemical functional groups of which the inhibitor is composed:

$$\log[K_i(i)] = \sum_j f_j \log[\kappa_i(j)] \quad (1)$$

where f_j is equal to 1/2 or 1/3 for nucleotide inhibitors that comprise two or three functional moieties (j), respectively. All of the nucleotide inhibitors in the data set contain at least two independent components: a nucleoside moiety and a (poly)phosphate group. A 2′(3′)-*O*-ribosyl substituent constitutes the third functional component that is present in most of the inhibitors in the data set. The $\kappa_i(j)$ comprise a set of 13 independent variables, which, in combinations of two or three, describe all members of the experimental data set. Five components, $\kappa_i(j)$, correspond to contributions from possible phosphate functional groups (mono-, di-, tri-phosphate, γ-[thio]triphosphate, and (βγ-imidino)triphosphate), six to nucleoside moieties (adenine, guanine, cytidine, uracil, hypoxanthine, and xanthine nucleoside), and two contributions to the 2′(3′)-*O*-ribosyl substituents, MANT and TNP. K_i values for 20 inhibitors were experimentally determined in this study, or in published work (Table S1). The experimental data set of inhibition constants for 20 compounds was modeled in a system of 20 equations (eq. 1) in 2 to 3 of 13 variables, as follows:

$$\log[K_i(\text{MANT-ATP})] = 1/3\,(\log[\kappa_i(\text{A})] + \log[\kappa_i(\text{MANT})] + \log[\kappa_i(\text{PPP})])$$

$$\log[K_i(\text{MANT-GTP}\gamma\text{S})] = 1/3\,(\log[\kappa_i(\text{G})] + \log[\kappa_i(\text{MANT})] + \log[\kappa_i(\text{PPSP})])] \quad (2)$$

$$\log[K_i(\text{TNP-ADP})] = 1/3\,(\log[\kappa_i(\text{A})] + \log[\kappa_i(\text{TNP})] + \log[\kappa_i(\text{PP})])$$

Least-squares fit of the 13 κ_i values to eq. 2 was carried out by singular value decomposition (SVD) (Press et al., 1992; Gray, 1997). The data matrix was decomposed as the product of two orthonormal matrices and a pseudo-diagonal matrix. Equation 1 was recast as $\log[K_i(i)] = N_{ij}\,\Sigma\,\log[\kappa_i(j)]$, where $K_i(i)$, i = 1 to 20, are the measured AC inhibition K_i values for the 20 dependent inhibitors, the $\kappa_i(j)$ are the values of two or three of the possible 13 independent components that constitute compound (i), and the elements N_{ij} are set to 1 if the jth independent component is present in the ith inhibitor and to 0 otherwise. SVD of N_{ij}/σ_i gives USV^t (σ_i is the standard deviation of $\log[K_i(i)]$ derived from nonlinear regression of $\log[K_i(i)]$ versus AC activity. It is noted that 20% of $\log[K_i]$ value was used as standard deviation for those inhibitors from Gille et al. (2004). S is a diagonal $j \times j$ matrix of singular values for the set of independent components. The columns of the 20 × j matrix U are orthonormal basis vectors that together with the significant values of S and the corresponding rows of the $j \times j$ matrix V^t (where t denotes the transpose) provide the best least-squares approximation to the original matrix N_{ij}/σ_i. The

values of $\log[\kappa_i(j)]$ were obtained from $\log[\kappa_i(j)] = (VS^+U^t) \times \log[K_i(i)]/\sigma_i$, as described previously (Press et al., 1992; Mou et al., 1999). Finally, substituting these values in eq. 2 gave the best-fit independent component values for the 13 values of $\log[\kappa_i(j)]$, from which calculated $K_i(i)$ were obtained. These best-fit values could be compared with the experimentally determined $K_i(i)$ values. A statistical test of the fit of the models is given by the probability Q (Press et al., 1992) that the χ^2 value (where $\chi^2 = \Sigma_i|(\log[K_{i\text{meas}}(i)] - \log[K_{i\text{calc}}(i)])/\sigma_i|^2$) from the fit to the data would be larger by chance. A larger value of Q indicates a better fit. Values of $Q > 0.1$ are adequate and may be acceptable above 0.001 (Press et al., 1992).

Results

Inhibition of VC1:IIC2 by MANT Nucleotides and TNP Nucleotides. As was reported previously (Gille et al., 2004; Mou et al., 2005), MANT-ATP and MANT-GTP inhibited the catalytic activity of VC1:IIC2 that was maximally stimulated by FSK, GTPγS-bound $G\alpha_s$ and Mn^{2+}, with K_i values in the 10 nM range (Table 1). However, when the linker between the MANT group and the ribosyl moiety was elongated to an aminoethyl-carbamoyl group, inhibitor potency at the fully activated VC1:IIC2 enzyme decreased approximately 500-fold. Translocation of the MANT group from the 2′,3′-*O*-ribosyl position to the N6-position (6-MANT-ATP) or N8 position (MABA-ATP and MAHA-ATP) of the adenine ring was also poorly tolerated in terms of potency. Extension of the linker between the adenine ring and MANT from butyl to hexyl (MABA-ATP→MAHA-ATP) was particularly detrimental to inhibitor potency.

TNP nucleotide triphosphates are moderately potent inhibitors of VC1:IIC2, with K_i values in the 100 nM range (Table 1). Like 2′,3′-MANT nucleotides, 2′,3′-TNP nucleotides are fluorescent (Hiratsuka, 2003). However, a major difference between MANT- and TNP nucleotides is that the TNP group is linked to both the 2′- and 3′-*O*-ribosyl atoms, preventing isomerization of the fluorophore and yielding a more defined but also more rigid molecule. Compared with MANT-ATP and MANT-GTP, TNP-ATP and TNP-GTP were approximately 7-fold less potent inhibitors of the fully activated VC1:IIC2 enzyme. Nonetheless, given their rigid structures, the potency of TNP-ATP and TNP-GTP was still very remarkable. In fact, the affinity of TNP-ATP and TNP-GTP for VC1:IIC2 is among the highest reported for targets of TNP nucleotides (Hiratsuka, 2003). It was also very remarkable that the pyrimidine nucleotide TNP-UTP exhibited nearly the same affinity for VC1:IIC2 as the purine nucleotides TNP-ATP and TNP-GTP. Exchange of uracil for cytidine, another pyrimidine base, reduced inhibitor potency 3-fold; nonetheless, the affinity of TNP-CTP for VC1:IIC2 surpassed that of TNP nucleotides for most other known target proteins (Hiratsuka, 2003). Elimination of the γ-phosphate in TNP-ATP, yielding TNP-ADP, reduced inhibitor-affinity 16-fold, and the elimination of the β-phosphate, yielding TNP-AMP, reduced inhibitor-affinity by an additional 13-fold. For TNP-GTP, the effect of elimination of the γ-phosphate was even more pronounced, with a 100-fold reduction in affinity.

TABLE 1

Inhibition of the catalytic activity of VC1:IIC2 by various MANT-nucleotides and TNP-nucleotides

The catalytic activity of VC1:IIC2 was determined in the presence of 10 mM $MnCl_2$ and 100 μM FSK in the absence or presence of GTPγS-activated $G\alpha_s$ as described under *Materials and Methods*. Reaction mixtures contained 40 μM ATP/Mn^{2+}, 1 μCi of [α-^{32}P]ATP, and TNP or MANT nucleotides at increasing concentrations to obtain saturated inhibition curves. K_i values were calculated from IC_{50} values using the previously published K_m values (Mou et al., 2005). Data shown are the means ± S.D. of three to six independent experiments performed in duplicate.

Nucleotide	K_i	
	VC1:IIC2 + FSK	VC1:IIC2 + FSK + $G\alpha_s$
	nM	*nM*
MANT nucleotides		
MANT-GTP	110 ± 19	11 ± 3.8
MANT-ATP	130 ± 11	14 ± 3.7
MANT-EDA-ATP	5500 ± 1100	6700 ± 890
6-MANT-ATP	11,000 ± 1900	9400 ± 1400
MABA-ATP	10,000 ± 1500	9400 ± 2100
MAHA-ATP	58,000 ± 12,000	100,000 ± 15,000
TNP nucleotides		
TNP-ATP	100 ± 30	81 ± 27
TNP-ADP	2000 ± 660	1300 ± 280
TNP-AMP	21,000 ± 7200	17,000 ± 6000
TNP-GTP	430 ± 130	83 ± 22
TNP-GDP	8100 ± 2900	9400 ± 1800
TNP-UTP	92 ± 9	92 ± 36
TNP-CTP	110 ± 16	310 ± 76

We also determined the potencies of nucleotides at inhibiting the submaximally activated VC1:IIC2 enzyme (i.e., the enzyme in the presence of FSK and Mn^{2+} but in the absence of activated $G\alpha_s$. Under these conditions, the potencies of MANT-GTP, MANT-ATP, and TNP-GTP were up to 10-fold lower, whereas the affinity of TNP-CTP was 3-fold higher. For the other nucleotides, the omission of activated $G\alpha_s$ had little effect on inhibitor potency.

Fluorescence Analysis of the Interaction of MANT-GTP and MANT-ATP with VC1:IIC2. In a previous study, we showed that the MANT group of MANT-GTP intercalates into a hydrophobic pocket between VC1 and IIC2, giving rise to increased nucleotide fluorescence at λ_{ex} = 350 nm (Mou et al., 2005). This fluorescence was further enhanced by the addition of the AC activator MP-FSK. Moreover, we observed FRET from Trp1020 of IIC2 to the MANT-group of MANT-GTP at λ_{ex} = 280 nm.

At λ_{ex} = 350 nm, both MANT-GTP and MANT-ATP were excited to emit light with a maximum at λ_{em} = 450 nm (Fig. 1, B and D). Upon addition of VC1:IIC2, the fluorescence of both MANT-GTP and MANT-ATP was increased, but the fluorescence increase with MANT-GTP was larger than with MANT-ATP. Addition of MP-FSK to samples further enhanced fluorescence; again, the fluorescence increase with MANT-GTP was larger than with MANT-ATP. Moreover, we noted that with MANT-GTP, the emission peak was shifted to shorter wavelengths than with MANT-ATP, indicating that the MANT group in MANT-GTP resided in a more hydrophobic environment than the MANT group of MANT-ATP (Mou et al., 2005).

As reported earlier (Mou et al., 2005), we observed FRET from Trp1020 of IIC2 to the MANT-group of MANT-GTP at λ_{ex} = 280 nm. At this wavelength, both MANT-GTP and MANT-ATP alone in solution showed only minimal fluorescence (Fig. 1, A and C). Upon addition of VC1:IIC2, large fluorescence signals with a peak at λ_{ex} = 350 nm were observed, corresponding to the endogenous tryptophan fluorescence of the protein. It should be noted that the shape of the emission spectra at λ_{ex} = 280 nm was different for MANT-GTP and MANT-ATP. In particular, the spectrum in the presence of MANT-ATP was steeper than in the presence of MANT-GTP (Fig. 1, compare green traces with the black

dashed lines showing endogenous VC1:IIC2 tryptophan fluorescence in the absence of MANT nucleotides). These data are indicative of FRET from Trp1020 of IIC2 to the MANT group of MANT-GTP, but not to the MANT group of MANT-ATP. Upon the addition of MP-FSK, the emission peak at λ_{em} = 350 nm was moderately decreased in the presence of MANT-GTP, and an additional fluorescence peak with a maximum at λ_{em} = 420 nm appeared. These data are indicative of enhanced FRET from Trp1020 to MANT-GTP. In contrast, only a very small decrease of the fluorescence peak at λ_{em} = 350 nm was observed upon the addition of MP-FSK to the MANT-ATP-inhibited enzyme, and there was virtually no fluorescence increase at λ_{em} = 420 nm, showing that FRET does not occur in this complex.

Crystal Structures of TNP-ATP·Mn^{2+} and MANT-ATP · Mn^{2+} Complexes. The similar inhibitory potencies of MANT-GTP and MANT-ATP toward VC1:IIC2 (Table 1), despite their different fluorescent properties upon interaction with VC1:IIC2 (Fig. 1), prompted us to compare the X-ray crystal structures of VC1:IIC2 bound to MANT-ATP with that of the complex of MANT-GTP, which was reported earlier (Mou et al., 2005). The remarkably high potencies of TNP nucleotides at inhibiting VC1:IIC2 (Table 1) led us to determine the X-ray crystal structure of VC1:IIC2 bound to TNP-ATP as well. Structures of $G\alpha_s$·GTPγS·VC1:IIC2·MP-FSK protein complexes with TNP-ATP·Mn^{2+} and MANT-ATP·Mn^{2+} were determined at 2.9- and 3.3-Å resolution, respectively. The $2|F_o| - |F_c|$ difference maps computed for crystals soaked in Mn^{2+} and TNP-ATP or MANT-ATP showed clearly interpretable electron density around the substrate-binding site (Fig. 2). Table 2 provides a summary of the crystallographic data collection and refinement statistics. The purine riboside and triphosphate moieties of both inhibitors occupy the same subsites observed for the corresponding groups of other ATP analogs (Tesmer et al., 1997, 1999, 2000), and their 2′,3′-ribosyl substituents bind to the previously recognized MANT binding pocket at the C1:C2 interface (Mou et al., 2005). Difference $|F_o| - |F_c|$ electron density for metal ions at the A and B sites is observed in both structures and is stronger than that in complexes in which only Mg^{2+} is present (data not shown), indicating that Mn^{2+} replaced Mg^{2+} at both sites. The two metal ions coordinate the 5′-triphosphates of 2′,3′-ribosyl-substituted ATP, and their protein ligands occupy roughly the same positions seen in complexes with MANT-GTP or un-/noncompetitive AC inhibitors (so-called P-site inhibitors) (Dessauer et al., 1999). However, the average temperature factors (B-factors) of TNP-ATP·Mn^{2+} and MANT-ATP·Mn^{2+} are 71 and 90 $Å^2$ and higher than those of the other ligands in the structure, MP-FSK and GTPγS, which are 34 and 41 $Å^2$, respectively. Therefore, we infer that the ATP analogs are less well ordered than the latter two ligands. Given the diffraction limits of the crystals of the two complexes, it is also possible that the high B-values reflect only partial occupancy of the catalytic site of C1:C2 by TNP-ATP and MANT-ATP. Because of the modest resolution of the data, combined with high B-factors of the ATP analogs, hydrogen bond interactions in the MANT-ATP·Mn^{2+}-bound complex cannot be unambiguously assigned.

We reported previously that the MANT fluorophore of MANT-GTP hampered the movement of the β1-α1-α2 loop of C1 and the α4′-β5′ and β7′-β8′ loops of C2 from the inactive (open) conformation to the active (closed) conformation (Mou et al., 2005) (Fig. 3, A and D). The TNP moiety of TNP-ATP (Figs. 2A and 3B) and the MANT substituent of MANT-ATP (Figs. 2B and 3C) occupy the same binding pocket at the C1:C2 interface and similarly prevent full domain closure. The overall pairwise root-mean-square deviations between corresponding Cα atoms of TNP-ATP·Mn^{2+}, MANT-ATP·Mn^{2+}, and MANT-GTP·Mn^{2+} complexes are less than 0.6 Å, suggesting that the global conformational differences among these inhibitor-bound complexes are small. However, relative to complexes with potent inhibitors, such as β-L-2′,3′-dideoxy-5′-ATP, the catalytic site, particularly the purine binding subsite, is slightly enlarged as a result of the intercalation of the MANT or TNP substituent between the C1 and C2 domains.

The conformations of TNP-ATP and MANT-ATP and their interactions with VC1:IIC2 residues in the substrate-binding site are illustrated in Fig. 3, B and C, respectively. The structure of the MANT-GTP·Mn^{2+} complex is also shown in Fig. 3D for comparison. The positions and orientations of 3′-MANT or 2′,3′-TNP substituents of ATP are similar to that of 3′-MANT of GTP in the binding groove between β1-α1-α2 of VC1 and α4′-β5′ of IIC2. The MANT groups of both MANT-ATP and MANT-GTP are in van der Waals contact with VC1 and IIC2 but do not form hydrogen bonds with neighboring protein residues. This binding pocket contains a group of conserved nonpolar residues including Trp1020 of

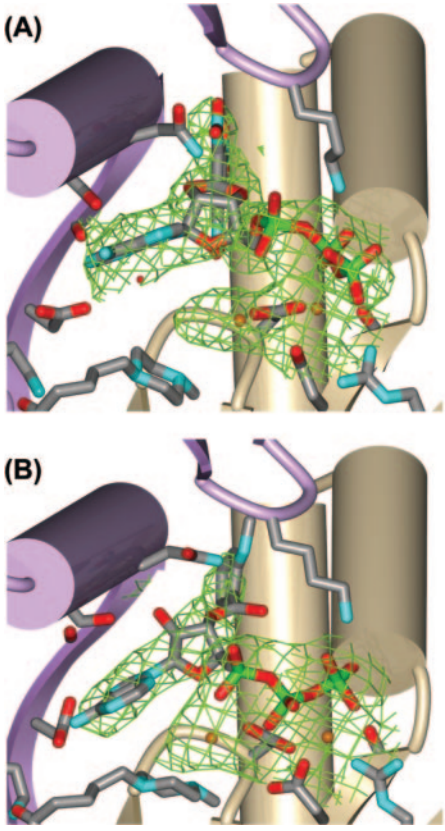

Fig. 2. Electron densities of TNP-ATP and MANT-ATP in the catalytic site of VC1:IIC2. The complexes formed with TNP-ATP (A) and MANT-ATP (B) in the presence of Mn^{2+} at 2.9- and 3.3-Å resolution, respectively. The models of the inhibitors are shown in ball-and–stick representation, and the individual electron density surrounding each ligand, shown in lime-green wire cage, is a $2|F_o| - |F_c|$ difference map calculated at the respective final resolution and contoured at the 1.2σ level.

IIC2 and two residues, Ala409 of VC1 and Ile1006 of IIC2, that are not conserved among the type I-VIII mAC isoforms (Mou et al., 2005). Substitution of Ala409 of VC1 with proline and/or Ile1006 of IIC2 with valine reduces the inhibitory potency of MANT-GTP to mAC by 2- to 10-fold, indicating that these nonconserved residues in the MANT binding pocket influence the affinity of mAC for inhibitors with 3′-MANT substituents. In the TNP-ATP·Mn^{2+} complex, the TNP substituent of ATP is bound to the same pocket that is occupied by the MANT group of the inhibitors described above. The two polar NH_2 groups of TNP seem to form hydrogen bonds with the carboximido NH_2 groups of Asn1022 and Asn1025 of IIC2 and the backbone oxygen of Ala409 of VC1 (Figs. 3B and 4E). These hydrogen bonds are presumed to stabilize the TNP ring in the VC1:IIC2 substrate-binding site.

The overall placement of the purine ring and 5′-triphosphate of TNP-ATP in the active site is similar to that of MANT-ATP (Figs. 2 and 3). Lys1029 from the α4 helix of IIC2 interacts with the nucleotide phosphates of analogs such as β-L-2′,3′-dideoxy-5′-ATP, which bind to and promote a fully closed conformation of the catalytic domain in which the C1 and C2 domains are in close opposition (Tesmer et al., 1999). This interaction cannot occur in the TNP- and MANT nucleotides because their 2′,3′-ribosyl substituents act as a wedge, preventing formation of the closed, active conformation (Fig. 3A).

The three derivatives differ greatly in the coordination of their poly-phosphate chains with neighboring protein residues and metal ions. In particular, the positions occupied by the β- and γ- phosphates of TNP-ATP are very close to those taken by the corresponding phosphates of β-L-2′,3′-dideoxy-5′-ATP and adenosine 5′-[α-thio]triphosphate but correspond to the binding sites of the α- and β-phosphates of MANT-ATP and MANT-GTP. As a result, Lys484 of VC1 can interact with the γ-phosphate of TNP-ATP (as in the complex with β-L-2′,3′-dideoxy-5′-ATP) but not with the γ-phosphate of MANT-GTP (Fig. 3, B–D). Lys1065 from β7′-β8′ of IIC2 interacts with a β-phosphate oxygen and the α-β bridging oxygen of TNP-ATP. The same interaction is observed with the corresponding atoms in the MANT-GTP complex (Fig. 3, B and D). Metal B is essential for stabilizing the ligand through an octahedral coordination with the oxygen atoms of two phosphates and three VC1 residues (Asp396, Ile397, and Asp440) in both TNP-ATP·Mn^{2+} and MANT-GTP·Mn^{2+} complexes (Fig. 2). Conversely, in the TNP-ATP·Mn^{2+} complex, metal A is coordinated by the two aspartate residues (Asp396 and Asp440) from VC1, but not with the α- or β-phosphates as observed in the MANT-GTP·Mn^{2+} complex (Figs. 2A and 3D). It should be noted that both TNP-ATP· Mn^{2+} and MANT-ATP·Mn^{2+} complexes were cocrystallized with MP-FSK rather than FSK. The 7-acetyl-7-[*O*-(*N*-methylpiperazino)-γ-butyryl] moiety of this ligand is bound closely to, but makes no direct contact with, the metal-A site (Figs. 2 and 3) in either structure.

The MANT and TNP nucleotide complexes show that the substrate-binding site of mAC is able to accommodate different purine substituents. It is remarkable that the purine moieties of TNP-ATP and MANT-ATP are bound to the same mAC subsite in completely different orientations (Fig. 4, A and D). The base of TNP-ATP adopts an *anti* conformation (χ = 234°) with respect to the ribose ring as observed for the guanine ring of MANT-GTP, but MANT-ATP adopts the *syn* orientation (χ = 64°), which is similar to that observed for other ATP analogs (Mou et al., 2005). Whereas the N6 and N7 atoms in the adenine ring of TNP-ATP form hydrogen bonds to Ser1028 of IIC2 (Fig. 3B), there are no apparent hydrogen bond interactions between the adenine ring of MANT-ATP and protein residues. The adenine moiety of MANT-ATP is observed at a position that is intermediate between the purine rings of MANT-GTP and TNP-ATP in the base-binding pocket (Fig. 4, A and D). Therefore, the potency for AC inhibitors containing 2′,3′-ribosyl substituents is not greatly determined by their nucleoside base, as is discussed below.

TABLE 2
Summary of crystallographic data collection and refinement statistics

Parameters	TNP-ATP:Mn	MANT−ATP:Mn
Cell constants (Å)		
a	118.2	116.8
b	133.4	132.1
c	70.6	69.6
No. of crystals	1	2
d_{min} (Å)	2.9	3.3
Avg. redundancy	4.3 (3.9)[a]	3.4 (1.7)
R_{sym}[b] (%)	17.6 (63.0)	16.2 (37.8)
Completeness (%)	82.5 (81.3)	85.8 (66.2)
$\langle I \rangle / \langle \sigma \rangle$	6.1 (1.2)	7.3 (1.4)
Resolution range for refinement[c] (Å)	15–2.9	15–3.3
Total reflections used	18,842	13,045
No. od protein atoms	5577	5589
No. od water molecules	51	0
No. od heterogen atoms	121	173
rmsd bond length (Å)	0.010	0.011
rmsd bond angle (°)	0.90	1.50
R_{work}[d] (%)	24.54	27.50
R_{free}[e] (%)	27.90	33.0
ave B − factor (Å^2)	44.9	51.4

[a] Numbers in parentheses refer to data in the highest resolution shell.
[b] $R_{sym} = \Sigma_h \Sigma |I(h) - I(h)_i| / \Sigma_h \Sigma_i I(h)_i$, where $I(h)$ is the mean intensity after rejections.
[c] Because of anisotropy, data with l index greater than 20 were omitted from refinement.
[d] $R_{work} = \Sigma_h ||F_o(h)| - |F_c(h)|| / \Sigma_h |F_o(h)|$, where $F_o(h)$ and $F_c(h)$ are observed and computed structure factors; no I/σ cutoff was used during refinement.
[e] Five percent of the complete data set was excluded from refinement to calculate R_{free}.

Discussion

The three independent X-ray crystal structures of VC1:IIC2 in complex with 2′,3′-ribose-substituted nucleotide AC inhibitors reported here and previously (Mou et al., 2005) reveal common features that we propose to be essential for their potency. A general tripartite pharmacophore model for catalytic site-targeted mAC inhibitors can be derived from the structural data and is supported by a systematic enzymatic analysis of natural and modified purine and pyrimidine nucleotides (Gille et al., 2004, 2005; Mou et al., 2005) (Fig. 4, B and C, and Table 1). The inhibitor site, which overlaps the binding site for the substrate ATP, contains a deep hydrophobic pocket for a 2′,3′ ribose substituent, a polar phosphate-binding groove adjacent to the catalytic Mn^{2+}-binding site, and a spacious base-binding pocket (Fig. 4A). Superposition of the three potent inhibitors MANT-GTP, TNP-ATP, and MANT-ATP in the AC substrate binding site (Fig. 4) shows that the ribose substituents and triphosphate

group (in coordination with two metal ions) are nearly aligned, but the base rings of these molecules are not.

Complementarity between the ribose-substituent and its binding pocket is essential for high-affinity binding. We previously showed that incorporation of a MANT group at the 3′-position of inosine 5′-[γ-thio]triphosphate increased inhibitory potency 60-fold (Gille et al., 2004). However, potency is decreased up to 40-fold relative to inosine 5′-[γ-thio]triphosphate when the ribose is substituted with a larger bulky BODIPY group, demonstrating the size-selectivity of the binding site for the ribose substituent of the inhibitor (Gille et al., 2004; Mou et al., 2005). In the present study, we show that substitution of UTP or CTP with 2′,3′-TNP increases the affinity of these pyrimidine nucleotides by up to 20,000-fold (Table 1) (Gille et al., 2005). Substitution of ATP with 2′,3′-aminoethyl-carbamoyl-MANT instead of MANT decreases potency up to 500-fold (Table 1), again confirming the size-selectivity of the pocket that accommodates the ribose substituent.

Several nonpolar residues conserved among mAC isoforms, including Trp1020 of IIC2, create a hydrophobic surface in the binding pocket for the ribose substituent (Mou et al., 2005). The increase in MANT fluorescence upon binding of MANT-GTP and MANT-ATP, or of FRET from MANT to Trp1020 (Fig. 1), is consistent with the interaction of the fluorophore with this hydrophobic pocket. Formation of hydrogen bonds between the NO_2 substituents of the trinitrophenyl group and polar groups in the binding site is probably crucial for the moderately high inhibitory potency of TNP-substituted nucleotides (Fig. 4E).

The nucleotide triphosphates that coordinate the two metal cofactors also provide substantial binding energy for interaction with VC1:IIC2. During catalysis, both metal ions play critical roles in ATP binding by coordinating the 3′-hydroxyl and 5′-triphosphate of ATP and neighboring protein residues around the catalytic core (Tesmer et al., 2000). Metal-B coordinates with the γ- and/or β-phosphate(s) of ATP analogs in the C1:C2 binding site (Tesmer et al., 1999, 2000; Mou et al., 2005) (Fig. 2B). Elimination of the γ-phosphate or β- and γ-phosphates of TNP-ATP reduce its affinity for VC1:IIC2 by approximately 20- and 200-fold, respectively (Table 1). The γ-phosphate is important for high binding affinity of TNP-GTP as well. The γ-phosphates of MANT-ATP and MANT-GTP also contribute at least 4-fold to their potency relative to the corresponding nucleotide diphosphates (Gille et al., 2004). The crystallographic data unequivocally dem-

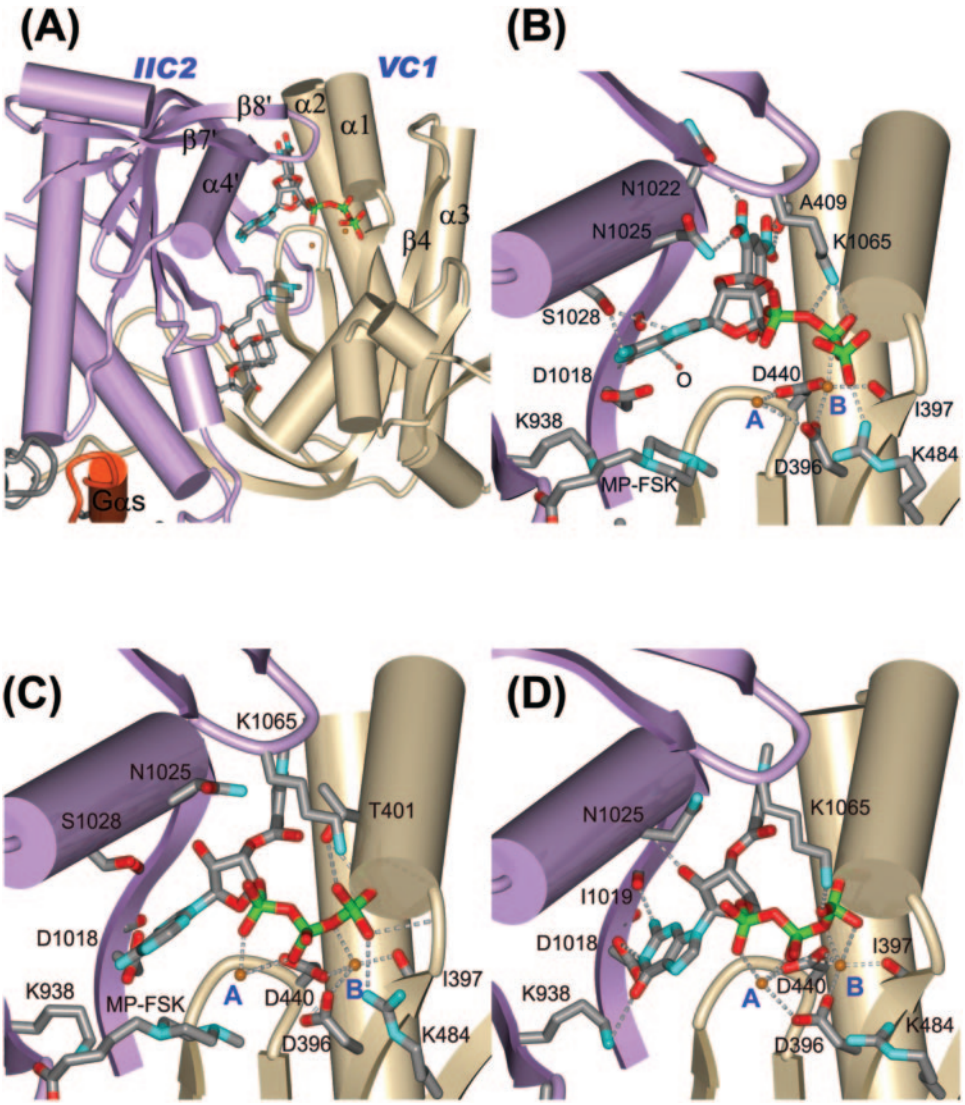

Fig. 3. Views of crystal structures of $G\alpha_s$·VC1·IIC2 in complex with substrate analogs. A, a wide-range view of complex of $G\alpha_s$-activated mAC with TNP-ATP and two Mn^{2+} ions in the catalytic site. VC1, IIC2, and $G\alpha_s$ are shown in mauve, tan, and gray, respectively. The α2 (switch II) helix of $G\alpha_s$ is shown in red. MP-FSK, TNP-ATP and two metal ions occupy the interdomain cleft between the C1 and C2 domains. Secondary structure elements are labeled as defined previously (Tesmer et al., 1997). Detailed views of the substrate-binding site of VC1·IIC2 showing TNP-ATP (B), MANT-ATP (C), and MANT-GTP (PDB 1TL7) (D) and two Mn^{2+} ions, respectively. MP-FSK and nucleotide inhibitors are drawn as stick models; carbon atoms are gray, nitrogen is blue, oxygen is red, and phosphorus is green; the two Mn^{2+} ions are shown as metallic orange spheres. Single-letter amino acid abbreviations are presented with position numbers, and protein residues are shown as stick models. The ribose substituents of inhibitor molecules are positioned between the α4 helix of IIC2 and α1-α2 helices of VC1. Interactions are shown among protein residues, inhibitors, and two metal ions in the VC1·IIC2 substrate-binding site. The gray dashed lines depict the hydrogen bonds between inhibitor molecules and protein residues, and coordination of the metal ions at sites A and B. Because of the high thermal parameters of the nucleotide (see text), hydrogen bond distances are approximate.

onstrate that the Mn^{2+} ion in the A-site coordinates with the α-phosphate of MANT-substituted nucleotides, but not with that of TNP-ATP (Fig. 2A). Therefore, at least one metal ion at B site is essential to coordinate and stabilize the polyphosphate chain in the binding groove.

The capacious subsite that accommodates the purine bases of MANT/TNP nucleotide inhibitors has little specificity; inhibitors with guanine, hypoxanthine and adenine bases have similar potency (Table 1) (Gille et al., 2004; Mou et al., 2005). Because the glycosidic angle has great rotational freedom, the orientation of the base is not restrained in these inhibitors. The structures of MANT/TNP nucleotide-VC1:IIC2 complexes show that the base rings of the inhibitor can be stabilized by different hydrogen bonding arrangements with the IIC2 purine-binding site depending on their orientation. In particular, the guanine ring of MANT-GTP and the adenine ring of P-site inhibitors are in opposite orientations, but maintain similar hydrogen bond pairs with Lys938, Asp1018, and Ile1019 from IIC2. The adenine ring of TNP-ATP adopts yet a different orientation in the binding pocket and forms a hydrogen bond with Ser1028 of IIC2 (Fig. 4D). However, in the context of other structural variations in the above three inhibitors, hydrogen bonds to the base seem to contribute little to interaction strength. The absence of base specificity for MANT or TNP-substituted purine nucleotides extends as well to their pyrimidine analogs. The inhibitory potencies of TNP-substituted pyrimidine nucleotides are at least comparable with, or even surpass those of, TNP-substituted purine nucleotides (Table 1). Nonetheless, bulky substitutions at various nitrogen atoms of the purine ring, such as those in 6-MANT-ATP, MABA-ATP, and MAHA-ATP, are not tolerated (Table 1), indicating that conformational flexibility of the purine-binding site of VC1:IIC2 is limited.

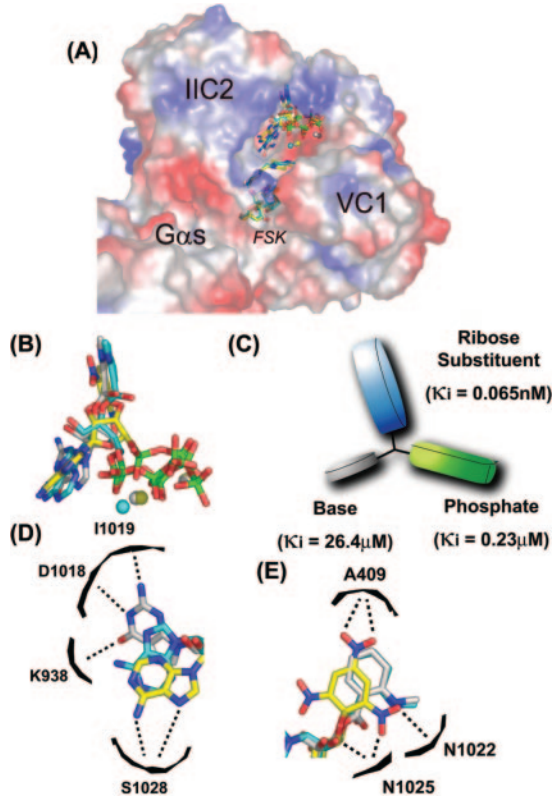

Fig. 4. General pharmacophore model of the mAC inhibitors. A, an overview of $G\alpha_s$·VC1:IIC2-inhibitor complexes, shown with the inhibitors superimposed. Carbon atoms are yellow for TNP-ATP, cyan for MANT-ATP, and gray for MANT-GTP in the VC1 and IIC2 protein interface. Mn^{2+} and FSK/MP-FSK are colored according to the respective ligand in the complex. Atoms are otherwise colored as described in the legend to Fig. 3. The molecular surface was calculated using the program PYMOL (DeLano Scientific, San Carlos, CA), based on the atomic coordinates of the $G\alpha_s$·VC1:IIC2·TNP-ATP complex. B, structures of MANT-ATP, MANT-GTP, and TNP-ATP, as bound to their respective complexes with $G\alpha_s$·VC1:IIC2 are superimposed and colored as in A. C, a general pharmacophore model of the mAC inhibitors from B with three functional groups, nucleotide base, blue; phosphate, green; 2′,(3′)-*O*-ribose substituent, gray. Overall κ_i values that represent the contribution of each type of functional group are indicated, computed from the mean of $\ln(\kappa_i)$ values for that group from Table 3. The latter were derived from SVD of the set of relationships given by eq. 1. The xanthine and monophosphate nucleotides were excluded from the averaging κ_i values for their apparently unfavorable contributions to the respective pharmacophore. D, a detailed schematic of base centers in the VC1:IIC2 purine-binding pocket. Hydrogen bonds between base (adenine group of TNP-ATP and guanine group of MANT-GTP) and neighboring IIC2 protein residues are shown in dashed lines. E, base substituent centers of inhibitors in the VC1:IIC2 substrate-binding site. Only the 2,4,6-trinitrophenyl substituent of TNP-ATP and the 2′-ribosyl OH of MANT-GTP form hydrogen bonds with VC1 and IIC2 protein residues.

We have used SVD to quantitatively compare the contributions to inhibitory potency from the independent functional groups in a set of 2′,3′-ribose-substituted nucleotide AC inhibitors. A relationship (eq. 1) was developed to express the K_i values of these compounds in terms of contributions from two to three chemical components corresponding to the base, phosphate, and 2′(3′)-*O*-ribosyl substituent. The data set of 20 inhibitors (Table 3) encompasses 13 variations of these three components (see *Materials and Methods*). SVD of the matrix of twenty equations corresponding to the inhibitor set (eq. 2) provides the least-squares fit of the observed K_i values to the thirteen independent affinity components κ_i that encompass the chemical variation among inhibitors. The κ_i values can be used to reconstitute computed K_i values that are comparable in magnitude with the observed set (Table 3; see Table 1 in the supplementary material). This analysis shows that the 2′(3′)-*O*-ribosyl substituent (MANT or NP) contributes 20-fold more to inhibitory potency than the phosphate group and nearly 1000-fold more than the base, as illustrated in the schematic shown in Fig. 4C. Although the data allowing comparison of the effects of MANT- and TNP-

TABLE 3
SVD analysis of the κ_i values for independent components from a set of AC inhibitors

Pharmacophore	Individual Component	κ_i[a]
		μM
Base	Adenine	2.9
	Guanine	48.9
	Cytidine	175
	Uracil	110
	Hypoxanthine	4.6
	Xanthine	247,000
Ribose substituent	MANT	$(0.0014 \pm 0.001) \times 10^{-3}$
	TNP	0.003
Phosphate	P	571,000
	PP	443
	PPP	0.06
	PPSP	0.45
	PPNP	0.48

P, monophosphate; PP, diphosphate; PPP, triphosphate; PPSP, [γ-thio]-triphosphate; and PPNP, [β,γ-imido]triphosphate.
[a] The best-fit κ_i values were derived from the experimental K_i values of 20 inhibitors (see *Material and Methods*) in the presence of FSK and GTPγS-activated $G\alpha_s$.

substitution of nucleotide di- and triphosphates are limited to adenine and guanine nucleotides (Table 1 of this study and Table 1 of Gille et al., 2004), it is evident that MANT substitution contributes more to potency than derivatization by TNP (Table 3).

Introduction of a bulky, aromatic group at the ribose 2′ and 3′ positions of ATP generates a class of mAC inhibitors that are resistant to hydrolysis and use a subsite at the interface of the C1 and C2 domains that is not present in the catalytically active conformation of the enzyme. The structures of complexes formed with such inhibitors indicate that the base-binding site is slightly enlarged, perhaps as a result of local distortions induced by binding of the MANT or TNP ribose substituent. Therefore, the specificity of base binding site for purines is relaxed relative to that of the active conformation of the enzyme, and specific interactions between the base and the base binding site have little influence on affinity for the inhibitor. For the MANT- and TNP-substituted nucleotides, binding energy not realized at the base binding site is recovered from interactions with the ribose substituent. Structures of a variety of C1:C2 complexes with ATP analogs and P-site inhibitors show that there is considerable variation in the mode of interaction between VC1:IIC2 and 5′- or 3′ phosphate groups and pyrophosphate, although similar patterns of metal cation and hydrogen bond recognition are observed in all complexes (Tesmer et al., 2000). The MANT/TNP nucleotide inhibitors take advantage of the plasticity of the phosphate binding site in forming interactions that optimize interactions at all subsites. Because mAC is deformable at the interface between its catalytic domains, the enzyme exhibits broad specificity for interaction with purine and pyrimidine nucleotides. MANT/TNP nucleotide inhibitors represent a novel class of potent mAC inhibitors in which relatively nonspecific yet energetically productive ionic van der Waals and hydrogen bonding interactions at three distinct subsites contribute to binding affinities in the 10 to 100 nM range. These compounds may be therefore viewed as lead compounds for the development of mAC isoform-specific, potent, and bioavailable inhibitors.

Acknowledgments

We thank Dr. Donald Gray and Tzu-Fang Lou (University of Texas at Dallas), and Arne Strand for extensive discussion on SVD calculations. We also thank the staff at the Advanced Light Synchrotron 8.2.1 beamline (Berkeley, CA) for their assistance with data collection.

References

Brunger AT, Adams PD, Clore GM, DeLano WL, Gros P, Grosse-Kunstleve RW, Jiang JS, Kuszewski J, Nilges M, Pannu NS, et al. (1998) Crystallography & NMR system: A new software suite for macromolecular structure determination. *Acta Crystallogr D Biol Crystallogr* **54:**905–921.

Dessauer CW, Scully TT, and Gilman AG (1997) Interactions of forskolin and ATP with the cytosolic domains of mammalian adenylyl cyclase. *J Biol Chem* **272:** 22272–22277.

Dessauer CW, Tesmer JJ, Sprang SR, and Gilman AG (1999) The interactions of adenylate cyclases with P-site inhibitors. *Trends Pharmacol Sci* **20:**205–210.

Gille A, Guo J, Mou TC, Doughty MB, Lushington GH, and Seifert R (2005) Differential interactions of G-proteins and adenylyl cyclase with nucleoside 5′-triphosphates, nucleoside 5′-[γ-thio]triphosphates and nucleoside 5′-[β,γ-imido]triphosphates. *Biochem Pharmacol* **71:**89–97.

Gille A, Lushington GH, Mou TC, Doughty MB, Johnson RA, and Seifert R (2004) Differential inhibition of adenylyl cyclase isoforms and soluble guanylyl cyclase by purine and pyrimidine nucleotides. *J Biol Chem* **279:**19955–19969.

Gille A and Seifert R (2003) 2′(3′)-*O*-(*N*-Methylanthraniloyl)-substituted GTP analogs: a novel class of potent competitive adenylyl cyclase inhibitors. *J Biol Chem* **278:**12672–12679.

Gray DM (1997) Derivation of nearest-neighbor properties from data on nucleic acid oligomers. II. Thermodynamic parameters of DNA.RNA hybrids and DNA duplexes. *Biopolymers* **42:**795–810.

Hanoune J and Defer N (2001) Regulation and role of adenylyl cyclase isoforms. *Annu Rev Pharmacol Toxicol* **41:**145–174.

Hiratsuka T (2003) Fluorescent and colored trinitrophenylated analogs of ATP and GTP. *Eur J Biochem* **270:**3479–3485.

Jones TA, Zou JY, Cowan SW, and Kjeldgaard (1991) Improved methods for building protein models in electron density maps and the location of errors in these models. *Acta Crystallogr A* **47:**110–119.

Linder ME, Ewald DA, Miller RJ, and Gilman AG (1990) Purification and characterization of $G_o\alpha$ and three types of $G_i\alpha$ after expression in *Escherichia coli*. *J Biol Chem* **265:**8243–8251.

Mou TC, Gille A, Fancy DA, Seifert R, and Sprang SR (2005) Structural basis for the inhibition of mammalian membrane adenylyl cyclase by 2′(3′)-*O*-(*N*-methylanthraniloyl)guanosine 5′-triphosphate. *J Biol Chem* **280:**7253–7261.

Mou TC, Gray CW, and Gray DM (1999) The binding affinity of Ff gene 5 protein depends on the nearest-neighbor composition of the ssDNA substrate. *Biophys J* **76:**1537–1551.

Otwinowski Z and Minor W (1997) Processing of X-ray diffraction data collected in oscillation mode. *Methods Enzymol* **276:**307–326.

Press WH, Teukolsky SA, Vetterling WT, and Flannery BP (1992) *Numerical Recipes in C,* 2nd ed, Cambridge University Press, New York.

Sunahara RK, Beuve A, Tesmer JJ, Sprang SR, Garbers DL, and Gilman AG (1998) Exchange of substrate and inhibitor specificities between adenylyl and guanylyl cyclases. *J Biol Chem* **273:**16332–16338.

Sunahara RK, Dessauer CW, and Gilman AG (1996) Complexity and diversity of mammalian adenylyl cyclases. *Annu Rev Pharmacol Toxicol* **36:**461–480.

Sunahara RK, Dessauer CW, Whisnant RE, Kleuss C, and Gilman AG (1997) Interaction of $G_s\alpha$ with the cytosolic domains of mammalian adenylyl cyclase. *J Biol Chem* **272:**22265–22271.

Tesmer JJ, Dessauer CW, Sunahara RK, Murray LD, Johnson RA, Gilman AG, and Sprang SR (2000) Molecular basis for P-site inhibition of adenylyl cyclase. *Biochemistry* **39:**14464–14471.

Tesmer JJ and Sprang SR (1998) The structure, catalytic mechanism and regulation of adenylyl cyclase. *Curr Opin Struct Biol* **8:**713–719.

Tesmer JJ, Sunahara RK, Fancy DA, Gilman AG, and Sprang SR (2002) Crystallization of complex between soluble domains of adenylyl cyclase and activated $G_s\alpha$. *Methods Enzymol* **345:**198–206.

Tesmer JJ, Sunahara RK, Gilman AG, and Sprang SR (1997) Crystal structure of the catalytic domains of adenylyl cyclase in a complex with $G_s\alpha$.GTPγS. *Science (Wash DC)* **278:**1907–1916.

Tesmer JJ, Sunahara RK, Johnson RA, Gosselin G, Gilman AG, and Sprang SR (1999) Two-metal-ion catalysis in adenylyl cyclase. *Science (Wash DC)* **285:**756–760.

Whisnant RE, Gilman AG, and Dessauer CW (1996) Interaction of the two cytosolic domains of mammalian adenylyl cyclase. *Proc Natl Acad Sci USA* **93:**6621–6625.

Address correspondence to: Dr. Stephen R. Sprang, Department of Biochemistry, The University of Texas Southwestern Medical Center at Dallas, Dallas, TX 75390-9050 E-mail: stephen.sprang@utsouthwestern.edu